Available online at www.sciencedirect.com
SCIENCE DIRECT®
Journal of Magnetic Resonance 166 (2004) 182–189
JMR Journal of Magnetic Resonance
www.elsevier.com/locate/jmr

MRI technique for measurement of velocity vectors, acceleration, and autocorrelation functions in turbulent flow

Andrew J. Sederman,* Mick D. Mantle, Craig Buckley, and Lynn F. Gladden

Department of Chemical Engineering, University of Cambridge, Pembroke Street, Cambridge, CB2 3RA, UK

Received 13 August 2003; revised 20 October 2003

Abstract

In this paper, we show velocity images for liquid flow in a cylindrical pipe at Reynolds numbers of up to 5000. Three orthogonal velocity components are acquired from a single excitation over a timescale of 60 ms thus obtaining an 'instantaneous' description of the fluid flow in steady laminar and chaotic turbulent flow. It is also shown how the technique, termed the gradient echo rapid velocity and acceleration imaging sequence (GERVAIS), can be used to acquire acceleration (convective derivative) images by incorporation of double pulsed gradient spin echo (PGSE) pairs into the pulse sequence such that the resulting phase shift is a measure of the change in the velocity over the mixing time between successive PGSE pairs. The technique has also been used to acquire up to 16 successive z-velocity images, providing spatio-temporal information of the velocity fluctuations over a period of 320 ms, which are then used to calculate spatially resolved velocity autocorrelation functions. It is found that over the timescale of the velocity measurements, which is principally determined by the residence time in the coil, the local velocity fluctuations are seen to be small compared to the local velocities, confirming that the data acquisition times achieved are rapid enough to capture 'instantaneous' images of the flow field.

Keywords: Magnetic resonance imaging; Turbulence; Velocity; Acceleration; Velocity autocorrelation

1. Introduction

To date, most quantitative MRI studies of liquid flow have addressed either steady-state flows or, in the case of non-steady state flows, have focused on negating or averaging the effects of variations in the fluid velocity so as to maximise the detected phase coherent magnetisation. Of course, whilst the acquired signal is maximised using such strategies, our ability to study the spatial and temporal correlations in the flow field is reduced. To achieve direct, quantitative measurement of spatio-temporal correlations in the flow requires data acquisition timescales that are rapid enough to capture instantaneous motion, i.e., th e sy stem remains steady during the time it takes to acquire a whole image; this precondition prohibits the use of most imaging techniques available.

Previous workers have investigated turbulent flow using a number of different approaches. Kuethe [1] reported the first imaging study of turbulent flow in which the flow was generated by a jet of water passing through a nozzle. In this study, a measure of turbulent diffusivity was obtained from a measurement of the signal attenuation observed in time-averaged images, employing an approach analogous to that of Stejskal and Tanner [2]. Again exploiting the phenomenon of signal loss as measured using a diffusion-weighted pulse sequence, Gatenby and Gore [3] used a spatially unresolved diffusion measurement sequence to study pipe flow up to Reynolds numbers as high as 6270. Using these data it was shown that the characteristic timescale of the velocity fluctuations was greater than the echo time employed in the experiment. A similar approach was used by Kuethe and Gao [4] to study pipe flows up to higher Reynolds numbers of 12,000–58,000. Li et al. [5] have reported time-averaged velocity measurements of flow in a cylindrical pipe; one-dimensional (1-D) velocity profiles were measured for Reynolds numbers up to 9000. These workers used a simple 1-D spin echo sequence with a set of velocity/phase encoding gradients

* Corresponding author. Fax: +441223766338.
E-mail address: ajs40@cheng.cam.ac.uk (A.J. Sederman).

1090-7807/$ - see front matter © 2003 Elsevier Inc. All rights reserved.
doi:10.1016/j.jmr.2003.10.016

placed either side of the π-refocusing pulse to measure the time-average velocity profiles and hence the average of the velocity fluctuations as a function of position. The results showed a correlation between the measured profile pixel intensity of the time-averaged flow image and the local turbulence intensity, with the latter showing good agreement with earlier data recorded using a hot-wire anemometer technique [6]. More recently, Han et al. [7] have used an approach similar to that of Li et al. [5] to investigate the non-Newtonian flow of blood in a pipe at Reynolds numbers up to 3500.

An alternative approach to addressing turbulent flows is based on echo-planar imaging (EPI) techniques. Kose [8–10] reported the first results of ultra-fast imaging of turbulent flow in which individual velocity vectors characterising the flow were resolved. In particular, Kose reported results from a one-shot velocity-mapping EPI sequence that was designed to acquire data in a short time compared to the velocity fluctuations (50–100 ms) occurring during flow at a Reynolds number of 2250. Two types of image were acquired, both employing a single r.f. excitation: (i) images of the v_z component of the flow, and (ii) two successive EPI images with a different velocity encoding between each image thereby yielding images of both v_x and v_y. In this latter case, the first image was preceded by an x-direction velocity encoding pair after which an x-unwind pair and a y-direction velocity encode pair were applied before the acquisition of the second image. Subsequent analysis of the data allowed the v_x and v_y component of the in-plane turbulent flow to be calculated. At a Reynolds number of 2250, on the cusp of the turbulent regime, vortices or eddies in the x,y-directions were observed to pass through the imaging volume. EPI velocity images of turbulent water flow up-stream and down-stream of an orifice plate were also presented. Various transverse images with the velocity-weighting gradient perpendicular and parallel to the axis of the pipe were taken at a series of axial distances along the pipe length. The velocity-weighted spin echo EPI sequence used allowed a 32×32 image (perpendicular to the direction of flow) to be acquired in 20.46 ms, with an echo time of 28 ms.

More recent work has again used standard EPI-based techniques to investigate local shear in the fluid flow, as determined by its influence on signal intensities in the image. In particular, Gatenby and Gore [11] used the theoretical formulation of the influence of shear on signal intensity reported by Kose [10], to characterise pipe flow using temporal and spatial intensity autocorrelation functions calculated from the experimental data.

In this paper we report, for the first time, the acquisition of three-component velocity images of turbulent flow in a pipe using an r.f. pulse sequence named the gradient echo rapid velocity and acceleration imaging sequence (GERVAIS). We also report how a modified EPI-based technique is implemented to acquire acceleration, or convective derivative, images and how spatially resolved temporal autocorrelation images of turbulent pipe flow are extracted from the data. Most importantly, the acceleration and, in particular, the temporal autocorrelation data demonstrate that the timescale of 60 ms required to acquire the three-component 2-D velocity image of turbulent flow up to the highest Reynolds number of 5000 studied here, is fast enough to record an 'instantaneous' image of the flow field. The temporal and spatial correlations observed in the flow field are consistent with the results of hot wire anemometry data [6], acquired under similar flow conditions.

Whilst our work is related to that of Kose a number of important differences and improvements exist in terms of both the implementation and design of the magnetic resonance (MR) pulse sequence and the physical nature of the flowing system. With respect to the development of the pulse sequence itself, we have incorporated subtle changes to Kose's original one-shot velocity EPI pulse sequence. First, an extra, orthogonal, velocity weighting gradient pair has been added to the EPI sequence that allows the acquisition of the full three-component velocity vector; previous results have only reported two components. Second, the acquisition of a train of velocity images from which a temporal correlation of the spatially resolved images is calculated, has demonstrated the validity of considering the data acquired using the GERVAIS pulse sequence as instantaneous images of the turbulent flow field at the Reynolds numbers investigated in this work. The maximum number of images acquired in this 'train' is determined by either fluid washout within the imaging coil or the timescale of relaxation of the spin system. Third, no velocity unwinding gradient is employed in GERVAIS and hence the phase shift measured, and also the resulting velocity image, will be influenced only by gradients applied in a single direction, thereby making the measurement of velocity in that direction more accurate. Avoiding use of an unwind gradient also removes errors in the velocity image due to changes in velocity over the duration of the image acquisition; such errors arise if the velocity is determined by the phase shift resulting from a wind-unwind pair. We note that the images of spatially resolved acceleration in the flow field reported in the present work confirm that any such 'errors' in a given velocity image acquired over the data acquisition timescales considered here will be small. However, in application to different systems, GERVAIS may offer significant advantages. Finally, fast gradient switching times and a larger acquisition bandwidth give a significant improvement in the acquisition time for a single image; image acquisition times being ~10 ms compared to ~20 ms in the previously published work. These image acquisition times have also been achieved for a larger data matrix of 64×32 compared with

32×32 reported in the earlier studies. The matrix size in the read direction is limited by a combination of the gradient strength, the acquisition bandwidth and the required signal-to-noise. In addition to the technical advances of the EPI-based MR pulse sequence we also show, for the first time, that the three velocity vectors can be acquired over a wide range of Reynolds numbers encompassing the transition from pure laminar flow into the fully turbulent flow regime ($1250 < Re < 5000$). Previous research in this area [8–10] was conducted at a single Reynolds number of 2250 which is at the transition of laminar flow to turbulent flow and not fully into the turbulent flow regime.

2. Experimental

MRI images of single-phase flow of a Newtonian fluid (water) in a long tube, in both the laminar and turbulent regime, were acquired using the GERVAIS pulse sequence.

2.1. MRI experimental

The GERVAIS pulse sequence used is shown in Fig. 1; pulse and delay timings are defined in this schematic. All experiments were performed on a Bruker DMX 200 vertical 149 mm bore spectrometer operating at a ^{1}H frequency of 199.7 MHz with a 64 mm diameter birdcage 'flow' probe which allowed full access from above and below the coil. Spatial resolution was achieved with a Bruker water-cooled 3-axis shielded gradient system capable of maximum field gradient strengths of 14 G cm^{-1} in conjunction with BAFPA 40 A amplifiers. Typical gradient rise times used were 50 μs; the actual value used was dependent on the gradient direction. The imaging section of GERVAIS is based on an MBEST-EPI [12] (or Blipped EPI) sequence with the addition that after the initial excitation pulse, each image is preceded by a velocity encoding gradient pair, separated by a 180° refocusing pulse. The velocity encoding gradient pair imparts a phase shift that is proportional to the velocity in the direction of the gradient. Further MBEST image acquisitions are then followed by a 180° refocusing r.f. pulse and the whole sequence is then repeated with appropriate choice of direction/magnitude of the velocity encoding pair. Hence, a series of images is acquired that have an additional phase shift due to motion in the direction of the applied velocity encoding gradients. The 180° pulse that follows each image acquisition helps to refocus some of the dephasing due to the inhomogeneous $\mathbf{B}_0$ field. Each velocity image is calculated from the phase shift between sequential images (or just the phase angle in the case of the first image after excitation) and therefore no phase rewind velocity gradient is required after each image acquisition. In practice, due to inherent phase shifts associated with the pulse sequence in the absence of flow, an experiment at zero liquid flow is also performed to calculate a "zero velocity" phase shift reference map which is then subtracted from the velocity phase shift image. The velocity is then quantified by calculation of the first moment of the velocity gradient [13]. All images were acquired with a field of view of 50 mm × 50 mm and 64 (read) × 32 (phase) points and a slice thickness of 1.7 mm. Typical pulse sequence parameters, as defined in Fig. 1, were as follows: Dwell time = 2.5 μs; δ = 1.1 ms; Δ = 3.45 ms; τ_m = 20 ms; $\mathbf{g}$ = 3.0–9.7 G cm^{-1};

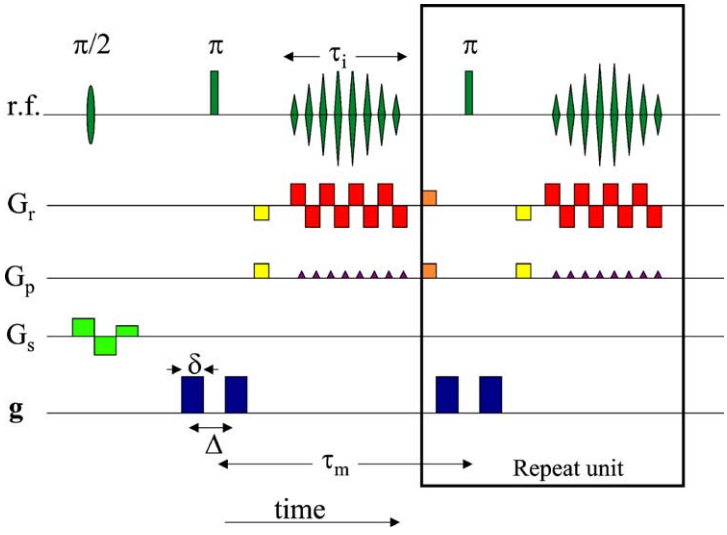

Fig. 1. Schematic of the GERVAIS pulse sequence, identifying all pulse and delay timings. The pulse sequence shown is that for acquisition of successive velocity images. The magnitude and orientation of the **g**-gradient are changed as determined by the velocity or acceleration vector that is to be measured. Pulse sequence parameters were as follows: Dwell time = 2.5 μs; δ = 1.1 ms; Δ = 3.45 ms; τ_m = 20 ms; $\mathbf{g}$ = 3.0–9.7 G cm^{-1}; duration of selective excitation pulse = 500 μs; duration of refocusing pulse = 230 μs.

duration of selective excitation pulse = 500 μs; duration of non-selective refocusing pulse = 230 μs. The slice gradient has been flow-compensated and the slice is selected towards the 'entrance' of the coil to minimise wash-out effects. The acquisition time for a single image, τ_i, is 10.2 ms with successive images being acquired in time intervals, τ_m, of 20 ms. Where the orientation of the velocity gradients is changed between image acquisitions, the superficial, z, direction was acquired last.

With reference to Fig. 1, the magnitude and orientation of the magnetic field gradients, **g**, are modified depending on the precise experiment being performed. When acquiring acceleration as opposed to velocity images, larger magnetic field gradients are used so as to obtain appreciable phase shifts in the acceleration image. As a result of this modification, the velocity image acquired after the first PGSE pair tends to suffer from severe aliasing and is also characterised by a poor signal-to-noise ratio where regions of high shear exist within a pixel. This latter effect arises because the large variation in velocity causes a large variation in phase shift, such that the resulting vector magnitude is small. However, these phase shifts are reversed by the second PGSE pair and therefore the second (acceleration) image does not suffer from such artefacts.

The experimental setup (i.e., flow in a cylindrical pipe) used in this study can in some ways be considered an 'ideal' system in that it is characterised by long relaxation times and has a simple geometry. Clearly, since GERVAIS is an EPI-based technique, T_2 relaxation times and $\mathbf{B_0}$ field homogeneity must be favourable for successful implementation. In recent studies we have successfully used GERVAIS to acquire 3 component velocity images for systems characterised by T_2 relaxation times as small as 50 ms. $\mathbf{B_0}$ homogeneity is critical to the quality of the results since a relatively small constant background gradient produces significant phase shifts at the highest velocities. Despite this, complex or structured media can be studied if care is taken to ensure sufficient $\mathbf{B_0}$ homogeneity (i.e., susceptibility matching). Effects of T_2 echo decay on image contrast have been dealt with by earlier workers [14]; since GERVAIS is a phase shift technique, such errors are expected to be small.

2.2. Experimental setup

All experiments were carried out in a straight smooth Perspex cylindrical tube of internal diameter 29 mm and length 3.1 m running through the bore of the magnet. Water (25 °C: density = 996 kg m^{-3}; viscosity 8.74×10^{-4} kg m^{-1} s^{-1}) was fed in to the tube from the top of the magnet. The imaging section was approximately 1.8 m from the tube inlet, between which there were no obstructions to the flow. The water was pumped using a Draper centrifugal pump through a flow controller and rotameter, and then through the magnet and back to the reservoir. $GdCl_3$ was added to the de-ionised water to reduce the longitudinal relaxation time to 500 ms such that a shorter recycle time could be used and the water in the imaging section of the magnet had spent sufficient time in the $\mathbf{B_0}$ field to allow near full T_1 relaxation. Superficial velocities were stepped up from 3.8 to 15.1 cm s^{-1} corresponding to Reynolds numbers up to 5000 (61 min^{-1}). Reynolds number, Re, is defined as

$$\mathrm{Re} = \frac{\rho v_{\mathrm{av}} d}{\mu}, \tag{1}$$

where ρ is the fluid density, v_{av} is the average fluid velocity in the direction of superficial flow, μ is the fluid dynamic viscosity, and d, is a characteristic length scale, in this case the internal diameter of the pipe.

3. Results and discussion

3.1. Three-component velocity imaging

One hundred and twenty eight images were acquired at each of 6 Reynolds numbers of 1250, 1700, 2500, 3300, 4200, and 5000, which corresponded to average liquid velocities of 3.8, 5.0, 7.5, 10.1, 12.6, and 15.1 cm s^{-1}, respectively. Fig. 2 shows samples of these three Cartesian component velocity images for each of the different liquid velocities. The velocity component in the superficial direction (v_z) is given by the colour scale bar and the magnitude and direction of the transverse (v_x, v_y) velocity components are indicated by the vector arrows present on each of the images. The total image acquisition time for each of these 3-component velocity images is 60 ms with each velocity component itself being acquired in <20 ms. In pipe flow, for a Newtonian fluid, the transition from laminar flow to turbulent flow is characterised by a Reynolds number of approximately Re = 2000 [15] though laminar regions may be observed up to Re = 4000. Figs. 2(A and B) show the flow profile when the Re is below this critical value. The theoretically predicted z-velocity profile for laminar flow (Re < 2000) of a Newtonian fluid is:

$$v_r = v_{\max}\left(1 - \frac{r^2}{a^2}\right), \tag{2}$$

where v_r is the z-velocity at radius r, v_{max} is the maximum (centreline) velocity and a is the pipe radius. A radial z-velocity profile taken across Fig. 2(A) and the fit to Eq. (2) are in good agreement as is shown in Fig. 3 for the case of flow at Re = 1250. The small asymmetry in the experimentally determined flow profile is most likely due to the finite entry-length of the pipe. In the laminar flow regime there should be no component of velocity in the x,y-directions as observed in Figs. 2(A and B). At Re = 2500 the flow is no longer fully laminar. There is a

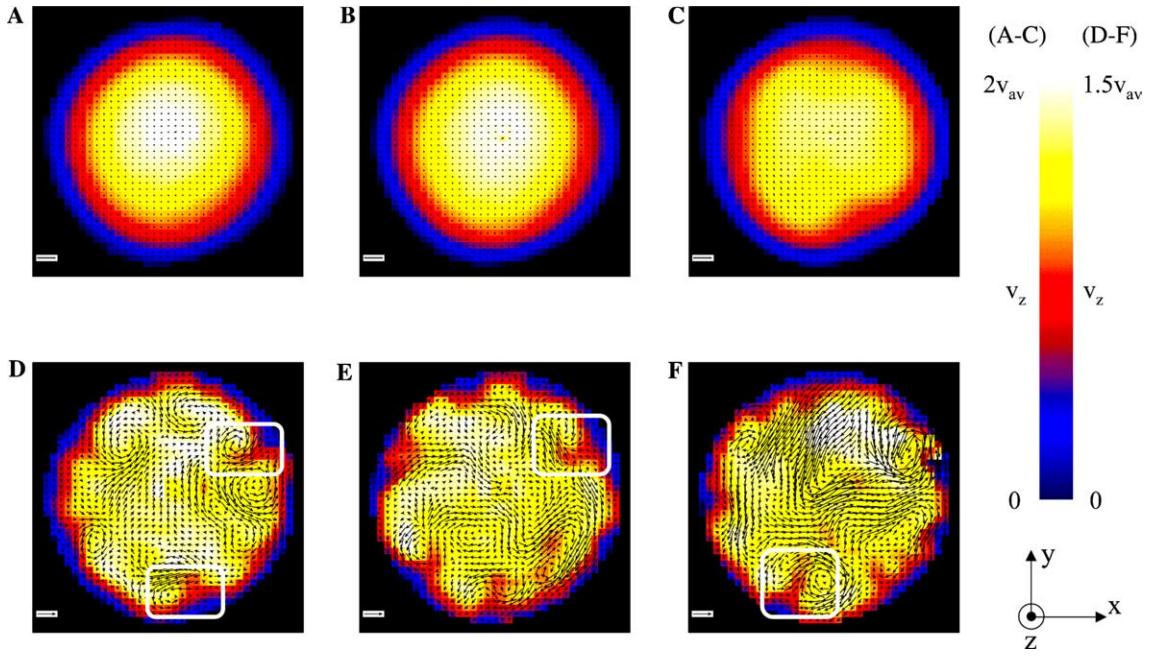

Fig. 2. Three orthogonal component velocity images acquired at increasing Re of (A) 1250, (B) 1700, (C) 2500, (D) 3300, (E) 4200, and (F) 5000. The colour scale identifies the magnitude of the z-velocity, and ranges from zero to twice the average velocity for A–C and from zero to 1.5 times the average velocity for D–F. The flow velocity in the plane of the image (i.e., x–y) is shown by the vectors on each image. The vector scale bar on each image corresponds to $1\,\mathrm{cm\,s^{-1}}$.

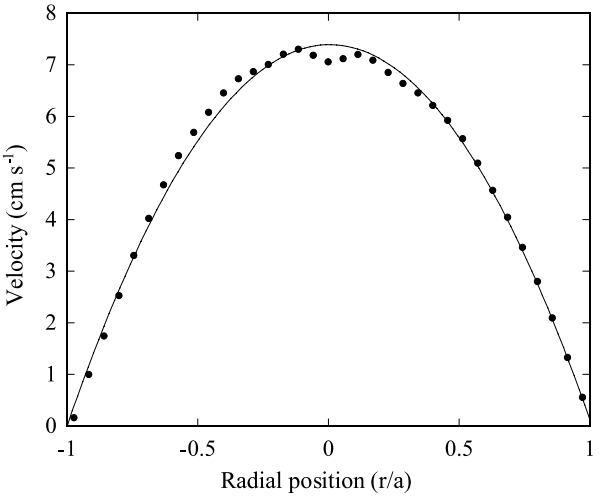

Fig. 3. Velocity profile at Re = 1250, as a function of dimensionless radial position. The theoretically predicted parabolic profile for laminar flow of a Newtonian fluid is shown by the solid line.

slight loss of symmetry and the profile is not parabolic. Instead there is a flattening of the profile at the centre of the pipe. It is also evident that, in the absence of turbulent 'puffs' [9,16], there are no significant x,y-velocities. For a small number of the velocity images recorded at Re = 2500, significant disturbances to the flow were observed in both the direction of superficial flow and the x,y-directions as turbulent puffs or eddies moved through the imaging section. This is likely to be due to the imperfection of the experimental set-up and the extreme non-linearity of the system such that a slight perturbation in the input parameters may cause a turbulent puff or eddy to form [16]. As Re is increased beyond the critical value, the flow becomes turbulent. These flow patterns can be qualitatively characterised by the following features:

- loss of radial symmetry and parabolic shape of the velocity profile
- chaotic flow evidenced by turbulent eddies
- high shear at the walls
- low z-velocity 'fingers' extending from the boundary layer at the pipe edge into the bulk fluid as indicated by the highlighted regions in Figs. 2(D–F).

Low z-velocity fingers are spatially correlated with both local high z-vorticity and transport away from the boundary layer, as evidenced by the x,y-velocities. With increasing Re all these characteristics remain, though more subtle differences are observed including higher magnitude velocity components in the x,y-velocity plane and a narrowing of the boundary layer.

Fig. 4 shows the azimuthally averaged radial profile of the flow velocity in the z-direction averaged over the 128 sets of images for each of the Reynolds numbers studied. Each profile has been normalised to the average velocity for each value of Re to obtain a dimensionless velocity, v/v_{av}, for easy comparison. As discussed earlier, the theoretically predicted half parabola is observed at low Re (<2000). As Re increases, the velocity profile in the centre of the pipe flattens off and with further

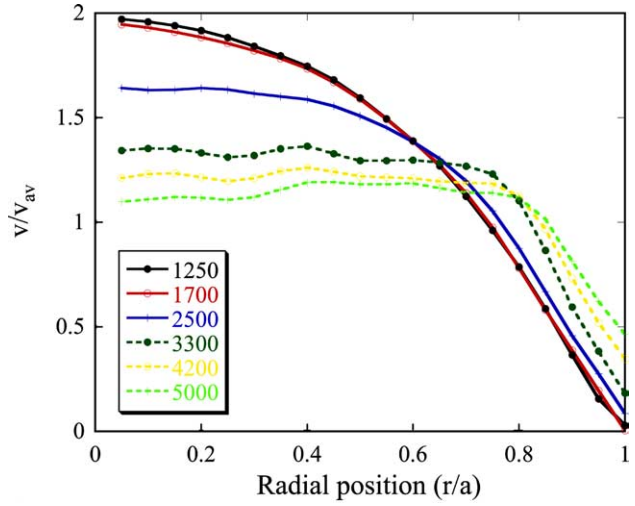

Fig. 4. Radial velocity profile of the z-velocity for Re in the range 1250–5000.

increases in Re the extent of plug flow increases, as identified by the constant velocity region in the normalised velocity profile. The measured velocity at the wall, non-zero due to the high shear rates and partial volume effects, also increases suggesting an increased shear rate at the pipe wall with increasing Re.

The following two sections report images of acceleration and velocity autocorrelation obtained using implementations of the GERVAIS pulse sequence. Whilst the ability to obtain these experimental data is of interest in its own right, both results also confirm that acquisition of the 2-D three-component velocity images has been achieved over a sufficiently fast timescale that the images shown in Fig. 2 can be considered an 'instantaneous' snapshot of the velocity field during turbulent flows up to the highest Reynolds number studied here.

3.2. Acceleration imaging

Acceleration, or convective derivative, images in the x- and z-direction are shown in Fig. 5 for Re = 5000. In both cases, the mixing time, τ_m, was 20 ms corresponding to the time between images such that the acceleration image is calculated from a change in velocity over τ_m using a methodology based on a double PGSE velocity gradient sequence [17]. These images correspond to a convective derivative because the data are essentially Lagrangian, i.e., moving in a frame of reference that follows the excited magnetisation with displacement in the image plane less than the pixel resolution, and will therefore represent the acceleration along the streamlines. In addition to demonstrating the ability to acquire images of acceleration directly, these data also confirm that changes in velocity over the timescale of acquiring the three-component velocity images, i.e., 40 ms between first and last velocity encoding pairs, are small compared to the overall velocities. In particular, for similar values of δ, Δ, $\mathbf{g}$ to those used in the velocity imaging pulse sequence and for $\tau_m = 20$ ms the maximum phase shifts are less than 10% of those in the velocity image corresponding to a maximum change in velocity of less than 10% of the maximum velocity during the acquisition time for a single velocity image.

3.3. Flow stability and the velocity autocorrelation function

The number of velocity images that can be acquired from a single excitation is generally limited by either the T_2 relaxation time or, in the case of this experimental setup, the fluid residence time in the coil. A series of 16 z-velocity images were acquired from a single excitation with a time increment of 20 ms between them. Fluid washout from the r.f. coil affected images acquired later in the image train, but even at the highest flow rate, the first 6 images were unaffected by this. If a series of velocity data are acquired over time the normalised velocity autocorrelation function (VACF), $R_v(\tau)$, can be calculated as:

$$R_v(\tau) = \frac{\langle v(t)v(t+\tau)\rangle}{\langle v^2\rangle}, \tag{3}$$

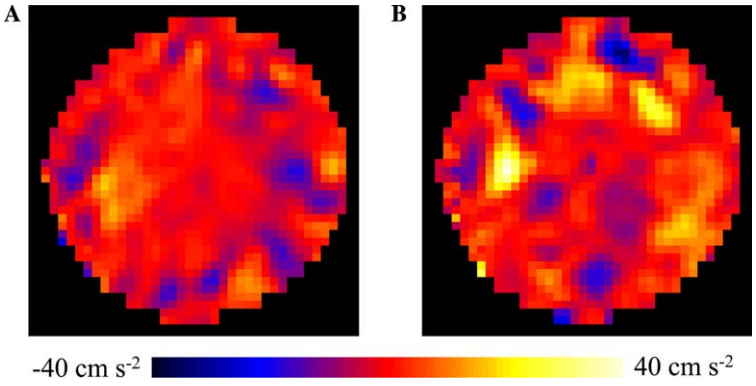

Fig. 5. Acceleration images in the (A) x-direction and (B) z-direction. Data are shown for liquid flow at Re = 5000, corresponding to an average superficial velocity of 15.1 cm s^{-1}.

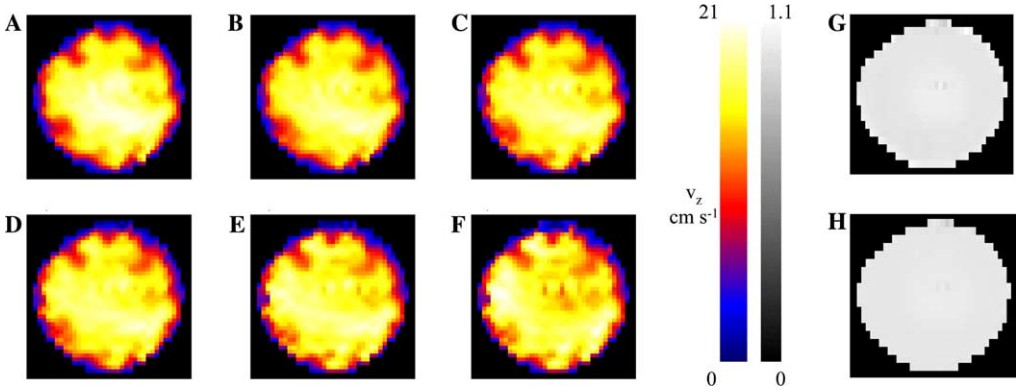

Fig. 6. Six consecutive z-velocity images acquired at 20 ms time intervals are shown (A–F) for flow at Re = 5000. The average VACF maps calculated from pairs of images separated by time intervals of (G) $\tau = 40$ ms and (H) $\tau = 80$ ms are also shown.

averaged over all t, where $v(t)$ is the local velocity at time, t [13,18]. When a series of velocity images are acquired, the spatially resolved temporal VACF is calculated by applying Eq. (3) on a pixel-by-pixel basis to produce a VACF map, two time delays, τ, of which are shown in Figs. 6(G and H). These data have been calculated from images obtained from 32 excitations (i.e., 192 images in total) so as to average over many different vortices and hence to produce a time-independent VACF. Again this will be essentially a Lagrangian VACF since the pulse sequence only refocuses signal that was initially excited by the $\pi/2$ pulse and in-plane displacements during data acquisition are less than the image resolution. In particular, Figs. 6(G and H) show the normalised average VACF at time intervals of 40 and 80 ms. These VACF maps are of uniform intensity corresponding to a numerical value of $\sim$1 with the standard deviation of values of the normalised VACF values within a map being less than 0.02. This analysis is consistent with there being only very small changes in the measured velocities over the timescales of 40 and 80 ms. Fig. 6 also shows 6 consecutive z-velocity images for Re = 5000. The images are acquired over 120 ms in total and show very little change between them with the low-velocity fingers extending from the wall remaining in the same position in each image. These images confirm the conclusion drawn from the VACF analysis and clearly illustrate that the timescale over which this series of images has been acquired does not exceed the eddy correlation time. These images also support the results obtained from the acceleration imaging experiments which showed that only small velocity changes are observed compared to the absolute velocity over these timescales. These result are important when assessing the extent to which the three-component velocity data shown in Fig. 2 can be considered an 'instantaneous' velocity measurement. The results shown in Fig. 6 clearly demonstrate that the timescale of changes in the velocity field occur over significantly longer timescales than 40 ms which is the time delay between applying the first and last set of velocity encoding gradients. Therefore, the images can be said to be 'instantaneous' or snapshot images of the turbulent flow field.

4. Conclusions

Three orthogonal component velocity imaging from a single excitation has been demonstrated for flow in a cylindrical pipe. Reynolds numbers in the range 1250–5000 have been studied and quantitative velocity profiles in laminar flow are shown to agree well with the theoretically predicted parabolic profile. In the turbulent regime, low z-velocity fingers extending from the walls toward the centre of the pipe were observed in addition to multiple turbulent puffs within a single image. These fingers were also often associated with in-plane motion away from the pipe wall into the bulk region. Acceleration, or convective derivative, imaging has been demonstrated by the use of a double PGSE sequence incorporated into the basic GERVAIS sequence, which confirmed that velocity variations are small over the timescale of the three-component imaging sequence.

The technique has also been used to acquire up to 16 velocity images at time intervals of 20 ms. The small changes seen over 40 and 80 ms in the spatially resolved velocity autocorrelation function calculated from these data confirm that the maximum duration between velocity encoding gradients of 40 ms used to acquire the full 2-D three-component flow image was sufficiently fast to capture an 'instantaneous' picture of the flow field up to the highest Reynolds number investigated here. The maximum timescale over which the spatially resolved velocity autocorrelation function can be calculated is limited by the residence time of the moving fluid within the imaging coil.

Acknowledgments

AJS and CB acknowledge EPSRC for financial support. LFG wishes to thank EPSRC for the award of the

NMR spectrometer. We also thank Paul Alexander for useful discussions.

References

[1] D.O. Kuethe, Measuring distributions of diffusivity in turbulent fluids with magnetic resonance imaging, Phys. Rev. A 40 (1989) 4542–4551.
[2] E.O. Stejskal, J.E. Tanner, Spin diffusion measurements: spin echoes in the presence of a time-dependent field gradient, J. Chem. Phys. 42 (1965) 288–292.
[3] J.C. Gatenby, J.C. Gore, Characterization of turbulent flows by NMR measurements with pulsed gradients, J. Magn. Reson. A 110 (1994) 26–32.
[4] D.O. Kuethe, J.H. Gao, NMR signal loss from turbulence—models of time-dependence compared with data, Phys. Rev. E 51 (1995) 3252–3262.
[5] T.Q. Li, J.D. Seymour, R.L. Powell, K.L. McCarthy, L. Ödberg, M.J. McCarthy, Turbulent pipe flow studied by time-averaged NMR imaging: measurements of velocity profile and turbulent intensity, Magn. Reson. Imaging 12 (1994) 923–934.
[6] J. Laufer, The structure of turbulence in fully developed pipe flow, NACA Report 1174 (1954) 1–18.
[7] S.-I. Han, O. Marseille, C. Gehlen, B. Blümich, Rheology of blood by NMR, J. Magn. Reson. 152 (2001) 87–94.
[8] K. Kose, Instantaneous flow-distribution measurements of the equilibrium turbulent region in a circular pipe using ultrafast NMR imaging, Phys. Rev. A 44 (1991) 2495–2504.
[9] K. Kose, One-shot velocity mapping using multiple spin-echo EPI and its application to turbulent flow, J. Magn. Reson. 92 (1991) 631–635.
[10] K. Kose, Visualization of local shearing motion in turbulent fluids using echo-planar imaging, J. Magn. Reson. 96 (1992) 596–603.
[11] J.C. Gatenby, J.C. Gore, Echo-planar-imaging studies of turbulent flow, J. Magn. Reson. A 121 (1996) 193–200.
[12] A.M. Howseman, M.K. Stehlingm, B. Chapman, R. Coxon, R. Turner, R.J. Ordidge, M.G. Cawley, P. Glover, P. Mansfield, R.E. Coupland, Improvements in snap-shot nuclear magnetic resonance imaging, Br. J. Radiol. 61 (1988) 822–828.
[13] P.T. Callaghan, Principles of Nuclear Magnetic Resonance Microscopy, Oxford University Press, New York, 1991.
[14] J. Hennig, k-space sampling strategies, Eur. Radiol. 9 (1999) 1020–1031.
[15] J.M. Coulson, J.F. Richardson, Chemical Engineering: Fluid Flow, Heat and Mass Transfer, Butterworth-Heinemann, Oxford, 1996.
[16] I.J. Wygnanski, M. Sokolov, D. Friedman, On transition in a pipe. Part 2 The equilibrium puff, J. Fluid Mech. 69 (1975) 283–304.
[17] P.T. Callaghan, S.L. Codd, J.D. Seymour, Spatial coherence phenomena arising from translational spin motion in gradient spin echo experiments, Concepts Magn. Reson. 11 (1999) 181–202.
[18] S. Stapf, Determination of velocity autocorrelation functions by multiple data acquisition in NMR pulsed-field gradient experiments, J. Magn. Reson. 152 (2001) 308–312.